JPET Fast Forward. Published on August 8, 2014 as DOI: 10.1124/jpet.114.215970
This article has not been copyedited and formatted. The final version may differ from this version.



# Quantitative prediction of transporter- and enzyme-mediated clinical drug-drug interactions of OATP1B1 substrates using a mechanistic net-effect model

Manthena V. Varma, Yi-an Bi, Emi Kimoto and Jian Lin

Pharmacokinetics Dynamics and Metabolism, Pfizer Global Research and Development, Pfizer Inc., Groton, CT 06340.

JPET Fast Forward. Published on August 8, 2014 as DOI: 10.1124/jpet.114.215970
This article has not been copyedited and formatted. The final version may differ from this version.



**Running title:** Mechanistic net-effect model for DDI predictions

**Corresponding Author:** Manthena V. Varma, Pharmacokinetics, Dynamics, and Metabolism, MS 8220-2451, Pfizer Global Research and Development, Pfizer Inc., Groton, CT 06340; Phone:+1-860-715-0257. Fax: +1-860-441-6402. E-mail: manthena.v.varma@pfizer.com

**Topic Category:** Metabolism, Transport and Pharmacogenomics

Number of text pages: 37

Number of tables: 2

Number of Figures: 4

Number of references: 48

Number of words in Abstract: 145

Number of words in Introduction: 570

Number of words in Discussion: 1745

**ABBREVIATIONS:** DDI, drug-drug interaction; CYP, Cytochrome P-450; OATP, organic anion transporting polypeptide; BCRP, breast cancer resistant protein; MRP, multidrug resistance protein; PBPK, physiologically-based pharmacokinetic; SCHH, sandwich culture human hepatocytes; AUCR, area under the plasma concentration-time curve ratio; $f_{u,b}$, fraction unbound in blood; Rb, blood-to-plasma ratio; $CL_{int,h}$, intrinsic hepatic clearance; Fa, fraction of drug absorbed; Fg, fraction of drug escaping gut-wall extraction; Fh, fraction of drug escaping hepatic extraction; $CL_h$, hepatic blood clearance; $CL_r$, renal clearance; $Q_h$, hepatic blood flow; $SF_{active}$, active uptake scaling factor; $PS_{active}$, sinusoidal active uptake clearance; $PS_{pd}$, passive diffusion; $CL_{int,bile}$, biliary intrinsic clearance; $CL_{int,CYP}$, metabolic intrinsic clearance; Ki, inhibition constant; $I_{u,max,in}$, maximum unbound concentration at the inlet to liver; $E_{max}$, maximum fold induction; $EC_{50}$, concentration of inducer associated with half-maximum induction; $I_{u,gut}$, free intestinal concentration; $I_{max,b}$, maximum total blood concentration; Ka, absorption rate constant; $f_{u,gut}$, fraction unbound in the gut; $Q_{gut}$, enterocytic blood flow; $CL_{r,sec}$, active renal secretion ; $Kp_{uu}$, liver-to-plasma unbound concentration ratio; RMSE, root mean square error; AFE, average fold error; FN, false negative.

JPET Fast Forward. Published on August 8, 2014 as DOI: 10.1124/jpet.114.215970
This article has not been copyedited and formatted. The final version may differ from this version.



**ABSTRACT**

Quantitative prediction of complex drug-drug interactions (DDIs) involving hepatic transporters and Cytochrome P-450s (CYPs) is challenging. We evaluated the extent of DDIs of nine victim drugs – which are substrates to organic anion transporting polypeptide 1B1 and undergo CYP metabolism or biliary elimination – caused by five perpetrator drugs, using *in vitro* data and the proposed 'extended net-effect' model. Hepatobiliary transport and metabolic clearance estimates were obtained from *in vitro* studies. Of the total of 62 clinical interaction combinations assessed using the net-effect model, 58 (94%) could be predicted within a 2-fold error, with few false negative predictions. Model predictive performance improved significantly when *in vitro* active uptake clearance was corrected to recover *in vivo* clearance. The basic R-value model yielded only 63% predictions within 2-fold error. This study demonstrates that the interactions involving transporter-enzyme interplay need to be mechanistically assessed for quantitative rationalization and prospective prediction.

## INTRODUCTION

The ability to quantitatively predict drug-drug interactions (DDIs) early in drug development is essential to minimize unexpected clinical study readouts and manage the adverse risks associated with drug interactions. Confidence in the prediction of DDIs for drugs eliminated via cytochrome-P-450 (CYP) enzymes is generally high (Obach et al., 2006; Fahmi et al., 2008). However, despite tremendous strides in several areas of drug transporters, reliable tools for quantitative prediction of transporter-based DDIs are not well established. In addition, significant challenges arise in the evaluation and/or prediction of complex drug interactions caused by perpetrator drugs and metabolites that affect multiple (transporter- and enzyme-mediated) disposition processes (Hinton et al., 2008; Yoshida et al., 2012).

In liver, organic anion transporting polypeptides (OATPs) OATP1B1, OATP1B3 and OATP2B1 are expressed on the sinusoidal membrane of hepatocytes and facilitate uptake of many clinically important anionic drugs, including HMG-CoA reductase inhibitors (statins) (Shitara and Sugiyama, 2006; Kalliokoski and Niemi, 2009; Giacomini et al., 2010; Fenner et al., 2012). Indeed, clinically relevant DDIs are attributed to the inhibition of transport mediated by members of the OATP family (Shitara et al., 2006). Furthermore, polymorphisms in *SLCO1B1* (encoding OATP1B1) were demonstrated with altered transporter activity leading to significant change in systemic exposure of statins; which could regulate relative peripheral tissue exposure and the risk of muscle toxicity (Nishizato et al., 2003; Niemi et al., 2005; Group et al., 2008; Ieiri et al., 2009). While hepatic uptake was suggested to be the rate-determining process in the systemic clearance of several OATP transporters substrates, including statins, enzymatic metabolism and/or biliary efflux also contribute to the systemic clearance and elimination from the body (Shitara et al., 2006; Watanabe et al., 2009; Maeda et al., 2011; Varma et al., 2012; Varma et al.,

2013a). For instance, atorvastatin is majorly metabolized by the CYP3A4, while repaglinide and cerivastatin are metabolized by CYP2C8 and CYP3A4. Canalicular efflux transporters, breast cancer resistant protein (BCRP) and multidrug resistance protein 2 (MRP2), are identified to be driving biliary elimination of rosuvastatin and pravastatin, respectively.

A conservative assessment of OATP-mediated DDIs can be made by a simplified static "R-value" model, which assumes active uptake solely contributing to clearance of the substrate "victim" drug (Giacomini et al., 2010; EMA, 2012; USFDA, 2012). However, lack of considerations to the quantitative contribution of the multiple disposition processes, R-value generally provides an oversimplification; and a predicted R-value>2 would generally require modeling in more refined static or dynamic models for quantitative DDI risk assessment and to evaluate the pharmacokinetic variability in the clinical studies. Recently, we reported the utility of the *in vitro* data to simulate pharmacokinetics of several OATP substrates using physiologically-based pharmacokinetic (PBPK) modelling (Varma et al., 2012; Varma et al., 2013a; Varma et al., 2013b). Our studies suggested that, for quantitative DDI predictions, the multiple components of transporter- and metabolic- clearance should be mechanistically considered.

The aim of the present study is to predict the transporter-based and complex DDIs of drugs with OATP-mediated hepatic uptake and CYP-mediated metabolism or biliary secretion. To achieve this, *in vitro* hepatobiliary transport metabolic rates were obtained and used, along with other input parameters, to quantitatively predict the change in systemic exposure using the proposed "extended net-effect" model (Varma et al., 2013b). This mechanistic model accounts for the simultaneous influence of reversible inhibition of active hepatic uptake and net-effect of

reversible inhibition, time-dependent inactivation and induction of CYPs in both the intestine and liver to quantitatively assess DDIs.

JPET Fast Forward. Published on August 8, 2014 as DOI: 10.1124/jpet.114.215970
This article has not been copyedited and formatted. The final version may differ from this version.



## MATERIALS AND METHODS

### Clinical DDI and *in vitro* data collection

Clinical DDI data of combinations involving nine victim drugs and 5 perpetrator drugs were primarily extracted from the University of Washington metabolism and transporter drug interaction database (www.druginteractioninfo.org). Additional exhaustive literature search was conducted to enrich the clinical DDI dataset. *In vitro* interaction potency data were collected from scientific literature. Corresponding references were cited in Supplementary material online.

### Transport studies using sandwich culture human hepatocytes (SCHH)

Cryopreserved human hepatocytes lot BD310 ( male donor) and lot 109 ( male donor) were purchased from BD Biosciences (Woburn, MA), and lot Hu4168 (female donor) was obtained from Life Technologies (Carlsbad, CA). Drugs substances were purchased from Sequoia Research Products (Pangbourne, UK) and Sigma-Aldrich (St. Louis, MO). All other chemicals were purchased from Sigma-Aldrich (St. Louis, MO). The SCHH methodology was described previously (Bi et al., 2006). Briefly, cryopreserved hepatocytes were thawed and plated with cell density of $0.75\times10^{6}$ cells/mL. The plates were overlaid with 0.25mg/ml matrigel on the second day and the cultures were maintained. On day 5, to determine the rates of uptake and passive diffusion, the cells were preincubated with or without 100 µM rifamycin SV, and to determine biliary clearance the cells were preincubated with or without $Ca^{++}$ HBSS buffer for 10 minutes. The reactions were initiated by addition of 1 µM victim drug and were terminated at predetermined time points by washing the cells three times with ice-cold HBSS. Cells were then lysed with 100% methanol containing internal standard and the samples were analyzed by LC-MS/MS (Supplementary material online).

JPET Fast Forward. Published on August 8, 2014 as DOI: 10.1124/jpet.114.215970
This article has not been copyedited and formatted. The final version may differ from this version.



**Static mechanistic "extended net-effect" model**

The area under the plasma concentration-time curve ratio (AUCR) of oral victim drug in the presence ($AUC'_{po}$) and absence ($AUC_{po}$) of perpetrator can be described by the following equations.

$$AUCR = \frac{AUC'_{po}}{AUC_{po}} = \frac{Fa'}{Fa} \cdot \frac{Fg'}{Fg} \cdot \frac{Fh'}{Fh} \cdot \frac{(CL_h + CL_r)}{(CL_h' + CL_r')} \quad (1)$$

$$Fh = 1 - \frac{CL_h}{Q_h} \quad (2)$$

$$CL_h = \frac{Q_h . f_{u,b} . CL_{int,h}}{Q_h + f_{u,b} . CL_{int,h}} \quad (3)$$

Fa, Fg, Fh represent the fraction of drug absorbed, fraction of drug escaping gut-wall extraction and hepatic extraction, respectively. Fa`, Fg`, Fh` are corresponding parameters in the presence of perpetrator. $CL_h$, $CL_r$, $CL_h$` and $CL_r$` represents hepatic and renal blood clearance in the absence and presence of the perpetrator, respectively. $CL_{int,h}$ is intrinsic hepatic clearance, $f_{u,b}$ is fraction unbound in blood, and $Q_h$ is hepatic blood flow (20.7 mL/min/kg (Kato et al., 2003)). Assuming no or negligible tubular reabsorption, renal clearance can be expressed as a function of glomerular filtration rate (GFR, 1.78 mL/min/kg) and active secretion ($CL_{r,sec}$).

$$CL_r = f_{u,b} . GFR + CL_{r,sec} \quad (4)$$

$CL_{int,h}$ is mathematically defined by extended clearance concept (further details in Supplementary online) (Liu and Pang, 2005; Shitara et al., 2006; Shitara and Sugiyama, 2006; Camenisch and Umehara, 2012; Barton et al., 2013; Li et al., 2014).

$$CL_{int,h} = \left(SF_{active} . PS_{active} + PS_{pd}\right) . \frac{\left(\sum CL_{int,CYP} + CL_{int,bile}\right)}{\left(PS_{pd} + \sum CL_{int,CYP} + CL_{int,bile}\right)} \quad (5)$$

JPET Fast Forward. Published on August 8, 2014 as DOI: 10.1124/jpet.114.215970
This article has not been copyedited and formatted. The final version may differ from this version.



$PS_{active}$ and $PS_{pd}$ are sinusoidal active uptake clearance and passive diffusion, respectively. Active uptake was assumed to be primarily OATP1B1-mediated transport. $CL_{int,bile}$ is biliary intrinsic clearance. $\sum CL_{int,CYP}$ represents the sum of intrinsic metabolic clearances by individual CYPs, and can also be expressed as: $CL_{int,met}.fm_{CYP\text{-}X} + CL_{int,met}.(1\text{-}fm_{CYP\text{-}X})$, where $CL_{int,met}$ is the total intrinsic metabolic clearance. $SF_{active}$ represents empirical scaling factor for active uptake estimated by matching the *in vitro* $CL_{int,h}$ (Eq. 5) to the *in vivo* $CL_{int,h}$, obtained from intravenous pharmacokinetics (Eq. 17). The *in vitro* intrinsic values were scaled assuming the following: $118x10^6$ hepatocytes $g^{-1}$ liver, 39.8 mg microsomal protein $g^{-1}$ liver, 24.5 g liver $kg^{-1}$ body weight (Varma et al., 2013b).

In the presence of perpetrator, the expected net-effect of reversible inhibition, time-dependent inhibition and induction, can be illustrated by,

$$CL_{int,h}' = \left( \frac{SF_{active} \,.\, PS_{active}}{RI_{OATP}} + PS_{pd} \right) \cdot \frac{\left( \sum \frac{CL_{int,CYP}}{RI_{h,CYP} \,.\, TDI_{h,CYP} \,.\, IND_{h,CYP}} + \frac{CL_{int,bile}}{RI_{efflux}} \right)}{\left( PS_{pd} + \sum \frac{CL_{int,CYP}}{RI_{h,CYP} \,.\, TDI_{h,CYP} \,.\, IND_{h,CYP}} + \frac{CL_{int,bile}}{RI_{efflux}} \right)} \qquad (6)$$

where $RI_{h,CYP}$ is the competitive inhibition term (Eq. 7), $TDI_{h,CYP}$ is the time-dependent inhibition term (Eq. 8) and $IND_{h,CYP}$ is the hepatic induction term (Eq. 9) for the interactions associated with the particular CYP isoform. These interaction terms will be reduced to one for enzymes not affected by the perpetrator and its metabolite. $RI_{OATP}$ is the competitive inhibition term (Eq. 7) for active hepatic uptake and $RI_{efflux}$ is the competitive inhibition term (Eq. 7) for biliary efflux transport (Fahmi et al., 2008; Giacomini et al., 2010; USFDA, 2012; Barton et al., 2013).

JPET Fast Forward. Published on August 8, 2014 as DOI: 10.1124/jpet.114.215970
This article has not been copyedited and formatted. The final version may differ from this version.



$$RI_{h,CYP} = 1 + \sum \frac{[I_{u,max,in}]}{Ki}; \quad RI_{OATP} = 1 + \sum \frac{[I_{u,max,in}]}{Ki_{OATP}}; \quad RI_{efflux} = 1 + \sum \frac{[I_{u,max,in}]}{Ki_{efflux}} \qquad (7)$$

$$TDI_{h,CYP} = \frac{k_{deg,h} + \frac{[I_{u,max,in}].k_{inact}}{[I_{u,max,in}] + K_I}}{k_{deg,h}} \qquad (8)$$

$$IND_{h,CYP} = \frac{1}{\left(1 + \frac{d.E_{max}.[I_{u,max,in}]}{[I_{u,max,in}] + EC_{50}}\right)} \qquad (9)$$

Ki is the inhibition constant and $I_{u,max,in}$ is the maximum unbound perpetrator concentration at the inlet to liver, calculated using Eq. 14. $K_{inact}$ and $K_I$ are maximal inactivation rate constant, respectively. $K_{deg,h}$ is the apparent first-order degradation rate constant of the affected enzyme. $E_{max}$ represent the maximum fold induction, and $EC_{50}$ is the concentration of inducer associated with half-maximum induction. The *d*-factor represents an empirical calibration factor for the *in vitro-in vivo* induction scaling, which was assumed to be one (USFDA, 2012; Einolf et al., 2014).

Assuming the gut metabolism is determined by only CYP3A4 (expression of other CYPs in the gut is negligible (Paine et al., 2006)) the change of the fraction of drug escaping intestinal extraction in the presence of perpetrator can be defined by Eq. 10 (Fahmi et al., 2008).

$$\frac{Fg'}{Fg} = \frac{1}{\frac{(1-Fg)}{RI_g \,.\, TDI_g . IND_g} + Fg} \qquad (10)$$

JPET Fast Forward. Published on August 8, 2014 as DOI: 10.1124/jpet.114.215970
This article has not been copyedited and formatted. The final version may differ from this version.



Where, $RI_g$, $TDI_g$ and $IND_g$ are the reversible inhibition (Eq. 11), time-dependent inhibition (Eq. 12) and induction (Eq. 13) terms for CYP3A4-mediated gut metabolism.

$$RI_g = 1 + \frac{[I_{u,gut}]}{Ki} \qquad (11)$$

$$TDI_g = \frac{k_{deg,g} + \frac{[I_{u,gut}] . k_{inact}}{[I_{u,gut}] + K_I}}{k_{deg,g}} \qquad (12)$$

$$IND_g = \frac{1}{\left(1 + \frac{d . E_{max} . [I_{u,gut}]}{[I_{u,gut}] + EC_{50}}\right)} \qquad (13)$$

$I_{u,gut}$, the free intestinal concentration of the perpetrator, was estimated by Eq. 15.

$$[I_{u,max,in}] = f_{u,b} \cdot \left([I_{max,b}] + \frac{Dose . Ka . Fa . Fg}{Q_h}\right) \qquad (14)$$

$$[I_{u,gut}] = \frac{Dose . Ka . Fa . f_{u,gut}}{Q_{gut}} \qquad (15)$$

Dose, $I_{max,b}$, Ka, $f_{u,gut}$ and $Q_{gut}$ (248 mL/min (Fahmi et al., 2008)) represent total dose given orally, maximum total blood concentration, absorption rate constant, fraction unbound in the gut and enterocytic blood flow, respectively. Consistent with the earlier reports, $K_{deg}$ was assumed to be $0.019h^{-1}$ for hepatic CYP3A4 and CYP2C8 and $0.029h^{-1}$ for intestinal CYP3A4 (Fahmi et al., 2008; Lai et al., 2009).

JPET Fast Forward. Published on August 8, 2014 as DOI: 10.1124/jpet.114.215970
This article has not been copyedited and formatted. The final version may differ from this version.



Change in active renal secretion ($CL`_{r,sec}$) caused by inhibition of OAT3 by gemfibrozil is described by a basic model (Feng et al., 2013).

$$CL_{r,sec}' = \frac{CL_{r,sec}}{\left(1 + \frac{I_{max,b} . f_{u,b}}{Ki_{OAT3}}\right)} \qquad (16)$$

*In vivo* $CL_{int,h}$ was calculated using the well-stirred liver model (Pang and Rowland, 1977).

$$CL_{int,h} = \frac{CL_h}{f_{u,b} \cdot \left(1 - \frac{CL_h}{Q_h}\right)} \qquad (17)$$

where $CL_h$ [= $(CL_p - CL_r)/Rb$] is the hepatic blood clearance obtained from intravenous total plasma clearance corrected for renal clearance and blood-to-plasma ratio (Rb).

$Kp_{uu}$ represent the unbound concentration in liver relative to the unbound concentration in plasma at steady state, given as (Liu and Pang, 2005; Shitara et al., 2006; Barton et al., 2013):

$$Kp_{uu} = \frac{SF_{active} . PS_{active} + PS_{pd}}{PS_{pd} + \sum CL_{int,CYP} + CL_{int,bile}} \qquad (18)$$

**Model Predictability**

All calculations were made using Microsoft Office Excel 2007. Prediction bias and precision were also assessed with root mean square error (RMSE) Eq. 19 and average fold error (AFE) Eq. 20.

$$RMSE = \sqrt{\frac{\sum(Predicted - Observed)^2}{N}} \qquad (19)$$

JPET Fast Forward. Published on August 8, 2014 as DOI: 10.1124/jpet.114.215970
This article has not been copyedited and formatted. The final version may differ from this version.



$$AFE = 10^{\frac{1}{N}\sum\left|\mathrm{Log}_{10}\frac{\mathrm{Predicted}}{\mathrm{Observed}}\right|} \qquad (20)$$

N is the number of observations.

## RESULTS

### *In vitro* hepatobiliary transport of OATP substrates

Active and passive hepatobiliary transport clearance of ten OATP1B1 substrates were determined *in vitro* using SCHH from three cyropreserved hepatocytes lots. All drugs showed active uptake – wherein rifamycin SV (100µmol/L) significantly ($p<0.05$) reduced their uptake into hepatocytes. On the other hand, biliary clearance is highest for fluvastatin and rosuvastatin with no or negligible secretion noted for cerivastatin, glyburide and repaglinide. All other input parameters, including metabolic intrinsic clearances, were obtained in-house or extracted from the literature reports (Table 1). The overall hepatic intrinsic clearance ($CL_{int,h}$), estimated assuming permeability-limited disposition using the "extended clearance" term (Eq. 5), however, underpredicted the *in vivo* hepatic clearance of all drugs except bosentan and glyburide (Figure 1A). Therefore, an empirical scaling factor for active uptake clearance ($SF_{active}$) was applied to scale-up the *in vitro* clearance to the *in vivo* hepatic clearance. The resulting geometric mean $SF_{active}$ of 10.6 recovered $CL_{int,h}$ for 6 of 10 (60%) drugs and 3-fold for 7 of 10 (70%) drugs within 2-fold (Figure 1B).

### Prediction of transporter- and enzyme-mediated DDIs

Clinical data of area under the plasma time-concentration curve (AUC) ratios (AUCR) of the OATPs substrates dosed with perpetrator drugs (cyclosporine, gemfibrozil, rifampicin, itraconazole and clarithromycin) were extracted from the published reports (Supplementary Table S1-S4). No clinical DDI report with these perpetrator drugs was available for valsartan, and thus the remaining nine drugs were considered for further DDI predictions. A total of 62 DDI combinations were evaluated with the proposed extended net-effect model, which captured

the intrinsic transport and metabolic clearance components of the victim drug and multiple interaction mechanisms of the perpetrator drug and its major circulating metabolite. Free drug hypothesis was assumed, and the DDI predictions are based primarily on the estimated free maximum perpetrator concentration in the gut ($I_{u,gut}$) and the inlet to liver ($I_{u,max,in}$).

Interactions with cyclosporine are evaluated assuming reversible inhibition of OATP1B1, MRP2, BCRP and CYP3A4 (Table 1). Predicted AUCRs were within 2-fold of the observed mean value for 10 of 12 (83%) cases, when using drug-specific $SF_{active}$ (Figure 2A and Supplementary Table S1). Precision and bias analysis of the cyclosporine DDIs yielded RMSE and AFE of 4.3 and 1.6, respectively (Table 2). Alternatively, R-value (Giacomini et al., 2010; EMA, 2012; USFDA, 2012) was calculated considering only OATP1B1 inhibition and compared to the predictions of current model. Although, the calculated R-value and the predicted AUCRs were similar in majority of the interactions with cyclosporine, R-value overpredicted (>2-fold error) exposure change in 25% cases (Figure 2A).

Interactions with gemfibrozil were evaluated, wherein gemfibrozil was assumed to reversibly inhibit OATP1B1, while its major circulating metabolite, gemfibrozil 1-*O*-$\beta$-glucuronide, cause reversible inhibition of OATP1B1 and time-dependent inhibition of CYP2C8. Additionally, inhibition of OAT3-mediated renal secretion of pravastatin and rosuvastatin was considered. Model predictions are within 2-fold error for 93% (14 of 15) cases, with RMSE and AFE of 2.6 and 1.4, respectively (Figure 2B and Table 2). On the other hand, R-value predicted only 46% interactions within 2-fold.

Rifampicin DDIs with victim drugs were well predicted (~95% within 2-fold), assuming OATP1B1 inhibition and/or CYP3A4 induction, on case basis (Figure 2C and Supplementary

JPET Fast Forward. Published on August 8, 2014 as DOI: 10.1124/jpet.114.215970
This article has not been copyedited and formatted. The final version may differ from this version.



Table S3). For instance, in DDI studies involving single concomitant dosing of victim drug and rifampicin, only OATP1B1 inhibition by rifampicin was considered. In contrary, where victim drug was dosed within 12.5h after the last dose of rifampicin chronic pre-treatment (5- or 7-day), both OATP1B1 inhibition and CYP3A4 induction activity were assumed simultaneously; while when dosed after 12.5h, only CYP3A4 induction was considered (Varma et al., 2013b). Incorporation of change in fraction escaping gut extraction (Fg), caused by CYP3A4 induction, significantly improved DDI predictions (Figure 2C). No considerable change in the predictions of rifampicin based DDIs were noted following sensitivity analysis to evaluate the effect of *d*-factor (Eq. 9) (Supplementary Figure S1).

All predicted AUCRs were within 2-fold for DDIs involving potent CYP3A4 inhibitors, itraconazole and clarithromycin (Figure 2D and Supplementary Table S4). In case of interactions with itraconazole, reversible inhibition of CYP3A4 by both parent and metabolite (4-hydroxyl itraconazole) was considered. On the other hand, clarithromycin showed moderate reversible inhibition of OATP1B1 and potent TDI of CYP3A4. RMSE and AFE were low (0.5 and 1.3, respectively), although 5 false negative predictions were noted with these perpetrator drugs (Table 2).

**Effect of $SF_{active}$ on AUCR prediction**

A comparison of the AUCR predictions assuming $SF_{active}$ of unity (no correction for *in vitro-in vivo* disconnect in $CL_{int,h}$), geometric mean of ten substrate drugs ($SF_{active}$ = 10.6) and drug-specific value, showed that the model predictability was lowest when the *in vitro* active rate was not corrected (Figure 3 and Table 2). Correspondingly, the model predictive performance was 63%, 86% and 94% (within 2-fold error), suggesting that correcting the active uptake rate not

JPET Fast Forward. Published on August 8, 2014 as DOI: 10.1124/jpet.114.215970
This article has not been copyedited and formatted. The final version may differ from this version.



only better recover the *in vivo* clearance of the victim drugs but also quantitatively explain their DDIs.

**Predicted change in free liver-to-plasma ratio ($Kp_{uu}$`/$Kp_{uu}$)**

To assess the change in free liver concentrations due to DDIs, free liver-to-plasma concentration ratio of the victim drug was calculated in the absence ($Kp_{uu}$) and presence ($Kp_{uu}$`) of perpetrator drug. The ratio of ratios ($Kp_{uu}$`/$Kp_{uu}$) indicated that inhibition of OATP1B1 by cyclosporine could reduce the $Kp_{uu}$ by ~75-90% (Figure 4). Gemfibrozil increased $Kp_{uu}$ at low doses, however, reduced the $Kp_{uu}$ by as much as ~75% at high doses. The simultaneous inhibition of OATP1B1-mediated uptake and induction of CYP3A4 activity following multiple-dose rifampicin treatment caused largest changes in $Kp_{uu}$ (~98% reduction). On the other hand, single dose rifampicin increased plasma AUC while decreasing $Kp_{uu}$. On the basis of the observed AUCRs and the predicted $Kp_{uu}$`/$Kp_{uu}$ ratios, the interactions were classified into four classes: Class-A interactions – increased systemic exposure and $Kp_{uu}$`/$Kp_{uu}$, Class-B interactions – increased systemic exposure and decreased $Kp_{uu}$`/$Kp_{uu}$, Class-C interactions – decreased systemic exposure and $Kp_{uu}$`/$Kp_{uu}$ and Class-D interactions – decreased systemic exposure and increased $Kp_{uu}$`/$Kp_{uu}$.

## DISCUSSION

This study demonstrated that the DDIs of OATP1B1 substrates involving transporter-enzyme interplay can be quantitatively predicted using the proposed static 'extended net-effect' model. The predictive evaluation not only considers multiple mechanisms of interaction of the perpetrator drug (and metabolite) simultaneously, but also captures the individual components of the overall clearance of the victim drug to evaluate transporter- mediated and complex-DDI situations. For a set of nine OATP1B1 substrates, 94% of the 62 combinations of clinical interactions with perpetrator drugs that affect OATP1B1 and/or CYPs activity were predicted within 2-fold error. Furthermore, the precision and bias analysis of whole dataset (RMSE and AFE of 2.4 and 1.4, respectively) suggested improved accuracy of the model compared to conventional models (eg. R-value).

The current SCHH data showed significant active transport for all victim drugs, which were also confirmed to be OATP1B1 substrates based on *in vitro* cellular uptake studies (data not shown). The hepatic clearance of the OATP1B1 substrates was considerably underpredicted, when estimated using *in vitro* metabolic/biliary intrinsic clearance alone, suggesting a key role of hepatic uptake in their disposition. The rate-determining role of the uptake transport for some of these drugs was also demonstrated in clinical studies and PBPK based assessments (Watanabe et al., 2009; Maeda et al., 2011; Jones et al., 2012; Jamei et al., 2013; Varma et al., 2013a; Varma et al., 2014). However, overall hepatic intrinsic clearance (calculated using Eq. 5) was underpredicted using the present *in vitro* transport and metabolic data, presumably due to discrepancy in the *in vitro-in vivo* extrapolation (IVIVE) of transporter-mediated uptake activity (Watanabe et al., 2009; Jones et al., 2012; Menochet et al., 2012; Varma et al., 2012; Jamei et al., 2013; Varma et al., 2013a). Therefore, an empirical scaling factor for active uptake ($SF_{active}$) was

applied to the extended clearance model (Eq. 5) to recover the observed *in vivo* clearance. Although, the individual scaling factors ranged from 1 (glyburide) to 101 (fluvastatin), the geometric mean $SF_{active}$ (10.6) recovered clearance for 60% and 70% of victim drugs within 2-fold and 3-fold, respectively (Figure 1B). With the three hepatocyte lots employed in this study, little inter-lot variability in active uptake was noted and no clear trend in lot-specific activity was observed (Figure 1), indicating that the *in vitro* underestimation of uptake clearance is consistent across hepatocyte lots. The potential reasons for the underestimation of the hepatic transporter activity may include down-regulation of transporter protein and/or partial loss of functional activity in the *in vitro* system (Watanabe et al., 2009; Jones et al., 2012; Menochet et al., 2012; Varma et al., 2012; Varma et al., 2013a). Based on the protein quantification using LC-MS/MS, our laboratory showed higher expression of OATPs in the human cryopreserved liver tissue in comparison to 5-day culture of SCHH – with an estimated relative expression factor (REF) of about 1.7-2.5 (Kimoto et al., 2012). However, REF only partially explains the scaling factor noted here. A recent report showed significant loss in transporter expression and activity in human cryopreserved hepatocytes compared to fresh hepatocytes and may contribute to the *in vitro-in vivo* disconnect (Lundquist et al., 2014). Genetic polymorphism in *SLCO1B1*, particularly homozygous OATP1B1*15 variant, was reported to possess reduced transport activity (Nishizato et al., 2003; Niemi et al., 2011; Lai et al., 2012; Tomita et al., 2013), and the hepatocytes with such variant may underpredict *in vivo* clearance. Further investigation in these areas is warranted to understand the lower functional activity in the *in vitro* systems (Barton et al., 2013; Zamek-Gliszczynski et al., 2013; Li et al., 2014; Lundquist et al., 2014). Nevertheless, improved DDI predictions with mean and drug-specific $SF_{active}$ (Figure 3) corroborate the

hypothesis of *in vitro-in vivo* discrepancy in transporter activity and justify the application of suggested correction factor ($SF_{active}$).

Multiple transporter and enzymes could be involved in the hepatic clearance for some of the victim drugs. For instance, rosuvastatin hepatic uptake was suggested to be mediated by OATP1B1, OATP1B3, OATP2B1 and NTCP (Kitamura et al., 2008; Bi et al., 2013). Considerations to the relative contributions are expected to yield improved predictions and can be incorporated in the current model. Here, we incorporated individual contribution of metabolic isozymes (CYP3A4, CYP2C8 and CYP2C9). However, due to the lack of definitive information for OATP isoforms for all the drugs, we assumed hepatic uptake is mediated only by OATP1B1. Generally, cyclosporine, gemfibrozil and rifampicin show similar inhibition potency ($IC_{50}$ or Ki values) for OATP1B1 and OATP1B3 (van Giersbergen et al., 2007; Gui et al., 2008; Gertz et al., 2013; Prueksaritanont et al., 2014), and therefore, AUCRs are not expected to be largely impacted by varied individual isoform contribution.

Interestingly, predicted change in overall hepatic clearance due to CYPs inhibition or induction was minimal compared with the change noted in gut extraction (Figure 2C and 2D). The differential impact of CYP3A4 inhibition on the gut extraction and overall hepatic clearance can be further exemplified with clinical observation of atorvastatin-itraconazole interactions – wherein intravenous itraconazole had no effect while oral itraconazole coadministration increased atorvastatin AUC significantly (Mazzu et al., 2000; Maeda et al., 2011). Presumably, hepatic uptake being the rate-determining step in the systemic clearance of several OATP substrates, change in only metabolic activity have a relatively smaller effect on the overall hepatic clearance, even for the drugs like atorvastatin, repaglinide and glyburide that are

completely metabolized (Maeda et al., 2011; Varma et al., 2013a; Varma et al., 2014). A systematic analysis suggested that inhibition of CYP3A4 or biliary clearance via MRP2 (pravastatin) and BCRP (rosuvastatin) alone by cyclosporine show no notable effect on the overall hepatic clearance and thus the AUCRs. Intestinal metabolism contributes to the first-pass extraction of drugs, particularly CYP3A substrates, and therefore, interactions at the level of the intestine are believed to be significant following oral dose (Bjornsson et al., 2003). In the current study, minimal or no change in gut extraction was predicted for the interactions with cyclosporine and gemfibrozil due to their weak interaction potency against CYP3A4 (Figure 2A and 2B). However, the prediction accuracy of the AUCRs with CYP3A inducer (rifampicin) and inhibitor (itraconazole and clarithromycin) was significantly improved after considering Fg`/Fg ratio in addition to the change in overall hepatic clearance (Figure 2C and 2D). Collectively, the model predictions suggest that the net effect of increased CYP3A activity at the gut and decreased hepatic uptake mainly determine the magnitude of interactions with rifampicin, while inhibition of CYP3A4 activity in the intestine contributes significantly to interactions with itraconazole.

Cyclosporine was suggested to increase oral absorption of certain drugs by inhibiting intestinal efflux transporters (P-gp, BCRP and MRP2), which may contribute to the observed AUCRs. However, due to complexity in the absorption kinetics, and lack of quantitative information on transporter expression and activity, change in Fa was not captured in the current model. Underprediction of pravastatin and rosuvastatin (BCS/BDDCS class 3 (Benet et al., 2011)) interactions with cyclosporine could be attributed to this (Varma et al., 2012; Jamei et al., 2013). Nevertheless, except for pravastatin and rosuvastatin, all victim drugs are highly permeable (as represented by class 1 and 2 of BCS/BDDCS) and efflux transporters has a minimal role in

limiting the intestinal absorption, while solubility may limit complete absorption of certain drugs. Previous reports considered Fa.Fg values of unity to predict inhibition DDIs (Yoshida et al., 2012). While this conservative approach is useful in avoiding false negatives predictions, this may result in overprediction of AUCR. Appropriate assessments of change in Fa may be derived based on PBPK models, which warrants further investigation and validation (Darwich et al., 2010; Fan et al., 2010).

For some of the victim drugs (eg. statins) free liver concentrations are key determinants of efficacy due to localization of pharmacological targets in the hepatocytes. Pharmacokinetic-pharmacodynamic relationships are typically established assuming plasma concentration mirror the intracellular concentration at target site, and therefore change in systemic pharmacokinetics is believed to translate to an equivalent effect on the target-site concentrations. However, OATPs substrates are highly concentrated in the liver and inhibition of hepatic uptake will have differential effects on plasma and liver concentrations. Although lack of clinical data would admittedly limit the validation, we predicted $Kp_{uu}$ in an attempt to assess the quantitative change in liver concentration in comparison to plasma concentration in several DDI situations. As noted here, except for DDIs associated with itraconazole and subtherapeutic doses of gemfibrozil (Class A), all the other interactions (Class B and C) result in a substantial drop in $Kp_{uu}$. These results have potential implications for clinical practice – particularly therapies using statins. Arguably, dose adjustments based on plasma exposure during co-medication may avoid systemic adverse events such as myopathy and rhabdomyolysis but could lead to lack of clinical efficacy due to reduced hepatic concentrations.

A strategy for model-based predictions of transporter- and complex-DDIs associated with transporter-enzyme interplay is proposed (Supplementary Figure S2). A conservative assessment

of hepatic transporter- or CYP-mediated DDIs for NCEs can be achieved with static basic models incorporating *in vitro* and *in vivo* drug parameters. The R-value generally provides an oversimplification of the transporter-mediated DDI risk, assuming hepatic active uptake is responsible for 100% of systemic clearance (Giacomini et al., 2010; USFDA, 2012). Therefore, a predicted positive R-value would require further assessment using mechanistic static or dynamic models for quantitative DDI evaluation. This study demonstrates the applicability of the static mechanistic model in the prediction of complex DDIs associated with multiple enzyme- and transporter-mediated processes. As shown here, hepatic transport kinetics and enzymatic (CYPs) stability data of the victim drug obtained from *in vitro* systems like SCHH and human liver microsomes can be used as inputs. However, due to the current knowledge gaps in the *in vitro-in vivo* extrapolation of uptake transporter kinetics, a scaling factor for active uptake may be needed to recover the *in vivo* intrinsic hepatic clearance – primarily assuming the metabolic/biliary clearance is accurately scalable. The scaling factor for active transport clearance can be derived based on intravenous or oral clinical pharmacokinetics data obtained early in the development (e.g. first-in-human study). However, when clinical pharmacokinetic data are not available the *in vitro* transport and metabolism data along with the validated geometric mean $SF_{active}$ may be employed for prospective predictions of transporter-mediated and complex-DDI situations. The drugs studied here are suggested *in vivo* probe drugs for testing clinical relevance of OATPs, CYP2C8 and CYP3A4 in the disposition of investigational drug (EMA, 2012; USFDA, 2012). With the comprehensive nature of the proposed static model, we note that the AUCRs predicted here are similar to those obtained by the dynamic mechanistic modeling (Varma et al., 2012; Jamei et al., 2013; Varma et al., 2013a; Varma et al., 2013b; Varma et al., 2014). The proposed static model has the advantage of being simple and more

transparent and can be valuable in quantitative predictions of DDI scenarios in the drug discovery and development.

In conclusion, where systemic clearance is determined by the hepatic uptake as well as metabolism or biliary secretion, mechanistic considerations assuming permeability-limited disposition and the simultaneous influence of all interaction mechanisms are needed to accurately predict transporter-mediated and complex DDIs. The proposed mechanistic model can be used for DDI risk assessment and potentially avoid unnecessary clinical DDI studies. Finally, this study mechanistically explained majority of the clinically relevant DDIs of statins and other OATP substrates.

JPET Fast Forward. Published on August 8, 2014 as DOI: 10.1124/jpet.114.215970
This article has not been copyedited and formatted. The final version may differ from this version.



**ACKNOWLEDGMENTS**

The authors would like to thank Mary Piotrowski for bioanalytical support. Authors would like to thank Larry Tremaine, R. Scott Obach, Odette Fahmi, Yurong Lai, Bo Feng, Theunis Goosen and Ayman El-Kattan for valuable inputs during this work.

**AUTHORSHIP CONTRIBUTIONS**

*Participated in research design:* Varma

*Conducted experiments:* Bi, Lin, Kimoto

*Contributed new reagents or analytic tools:* Varma

*Performed data analysis:* Varma, Lin, Bi

*Wrote or contributed to the writing of the manuscript:* Varma, Kimoto, Lin, Bi

## CONFLICT OF INTEREST

All authors are full-time employees of Pfizer Inc. The authors have no conflicts of interest that are directly relevant to this study.

## REFERENCES

Barton HA, Lai Y, Goosen TC, Jones HM, El-Kattan AF, Gosset JR, Lin J and Varma MV (2013) Model-based approaches to predict drug-drug interactions associated with hepatic uptake transporters: preclinical, clinical and beyond. *Expert Opin Drug Metab Toxicol* **9**:459-472.

Benet LZ, Broccatelli F and Oprea TI (2011) BDDCS applied to over 900 drugs. *The AAPS journal* **13**:519-547.

Bi YA, Kazolias D and Duignan DB (2006) Use of cryopreserved human hepatocytes in sandwich culture to measure hepatobiliary transport. *Drug Metab Dispos* **34**:1658-1665.

Bi YA, Qiu X, Rotter CJ, Kimoto E, Piotrowski M, Varma MV, Ei-Kattan AF and Lai Y (2013) Quantitative assessment of the contribution of sodium-dependent taurocholate co-transporting polypeptide (NTCP) to the hepatic uptake of rosuvastatin, pitavastatin and fluvastatin. *Biopharm Drug Dispos* **34**:452-461.

Bjornsson TD, Callaghan JT, Einolf HJ, Fischer V, Gan L, Grimm S, Kao J, King SP, Miwa G and Ni L (2003) The conduct of in vitro and in vivo drug-drug interaction studies: a Pharmaceutical Research and Manufacturers of America (PhRMA) perspective. *Drug Metabolism and Disposition* **31**:815-832.

Camenisch G and Umehara K (2012) Predicting human hepatic clearance from in vitro drug metabolism and transport data: a scientific and pharmaceutical perspective for assessing drug-drug interactions. *Biopharm Drug Dispos* **33**:179-194.

Darwich AS, Neuhoff S, Jamei M and Rostami-Hodjegan A (2010) Interplay of metabolism and transport in determining oral drug absorption and gut wall metabolism: a simulation assessment using the Advanced Dissolution, Absorption, Metabolism (ADAM) model. *Current drug metabolism* **11**:716-729.

Einolf HJ, Chen L, Fahmi OA, Gibson CR, Obach RS, Shebley M, Silva J, Sinz MW, Unadkat JD, Zhang L and Zhao P (2014) Evaluation of various static and dynamic modeling methods to predict clinical CYP3A induction using in vitro CYP3A4 mRNA induction data. *Clin Pharmacol Ther* **95**:179-188.

EMA (2012) Guideline on the Investigation of Drug Interactions. *Committee for Human Medicinal Products (CHMP).*

Fahmi OA, Maurer TS, Kish M, Cardenas E, Boldt S and Nettleton D (2008) A combined model for predicting CYP3A4 clinical net drug-drug interaction based on CYP3A4 inhibition, inactivation, and induction determined in vitro. *Drug Metab Dispos* **36**:1698-1708.

Fan J, Chen S, CY Chow E and Sandy Pang K (2010) PBPK modeling of intestinal and liver enzymes and transporters in drug absorption and sequential metabolism. *Current drug metabolism* **11**:743-761.

Feng B, Hurst S, Lu Y, Varma MV, Rotter CJ, El-Kattan A, Lockwood P and Corrigan B (2013) Quantitative prediction of renal transporter-mediated clinical drug-drug interactions. *Mol Pharm* **10**:4207-4215.

Fenner KS, Jones HM, Ullah M, Kempshall S, Dickins M, Lai Y, Morgan P and Barton HA (2012) The evolution of the OATP hepatic uptake transport protein family in DMPK sciences: from obscure liver transporters to key determinants of hepatobiliary clearance. *Xenobiotica* **42**:28-45.

Gertz M, Cartwright CM, Hobbs MJ, Kenworthy KE, Rowland M, Houston JB and Galetin A (2013) Cyclosporine inhibition of hepatic and intestinal CYP3A4, uptake and efflux transporters: Application of PBPK modeling in the assessment of drug-drug interaction potential. *Pharmaceutical research*:1-20.

Giacomini KM, Huang SM, Tweedie DJ, Benet LZ, Brouwer KL, Chu X, Dahlin A, Evers R, Fischer V, Hillgren KM, Hoffmaster KA, Ishikawa T, Keppler D, Kim RB, Lee CA, Niemi M, Polli JW, Sugiyama Y, Swaan PW, Ware JA, Wright SH, Yee SW, Zamek-Gliszczynski MJ and Zhang L (2010) Membrane transporters in drug development. *Nat Rev Drug Discov* **9**:215-236.

Group SC, Link E, Parish S, Armitage J, Bowman L, Heath S, Matsuda F, Gut I, Lathrop M and Collins R (2008) SLCO1B1 variants and statin-induced myopathy--a genomewide study. *N Engl J Med* **359**:789-799.

Gui C, Miao Y, Thompson L, Wahlgren B, Mock M, Stieger B and Hagenbuch B (2008) Effect of pregnane X receptor ligands on transport mediated by human OATP1B1 and OATP1B3. *Eur J Pharmacol* **584**:57-65.

Hinton LK, Galetin A and Houston JB (2008) Multiple inhibition mechanisms and prediction of drug-drug interactions: status of metabolism and transporter models as exemplified by gemfibrozil-drug interactions. *Pharm Res* **25**:1063-1074.

Ieiri I, Higuchi S and Sugiyama Y (2009) Genetic polymorphisms of uptake (OATP1B1, 1B3) and efflux (MRP2, BCRP) transporters: implications for inter-individual differences in the pharmacokinetics and pharmacodynamics of statins and other clinically relevant drugs. *Expert Opin Drug Metab Toxicol* **5**:703-729.

Jamei M, Bajot F, Neuhoff S, Barter Z, Yang J, Rostami-Hodjegan A and Rowland-Yeo K (2013) A Mechanistic Framework for In Vitro-In Vivo Extrapolation of Liver Membrane Transporters: Prediction of Drug-Drug Interaction Between Rosuvastatin and Cyclosporine. *Clin Pharmacokinet*.

Jones HM, Barton HA, Lai Y, Bi YA, Kimoto E, Kempshall S, Tate SC, El-Kattan A, Houston JB, Galetin A and Fenner KS (2012) Mechanistic pharmacokinetic modeling for the prediction of transporter-mediated disposition in humans from sandwich culture human hepatocyte data. *Drug Metab Dispos* **40**:1007-1017.

Kalliokoski A and Niemi M (2009) Impact of OATP transporters on pharmacokinetics. *Br J Pharmacol* **158**:693-705.

Kato M, Chiba K, Hisaka A, Ishigami M, Kayama M, Mizuno N, Nagata Y, Takakuwa S, Tsukamoto Y, Ueda K, Kusuhara H, Ito K and Sugiyama Y (2003) The intestinal first-pass metabolism of substrates of CYP3A4 and P-glycoprotein-quantitative analysis based on information from the literature. *Drug Metab Pharmacokinet* **18**:365-372.

Kimoto E, Yoshida K, Balogh LM, Bi YA, Maeda K, El-Kattan A, Sugiyama Y and Lai Y (2012) Characterization of organic anion transporting polypeptide (OATP) expression and its functional contribution to the uptake of substrates in human hepatocytes. *Mol Pharm* **9**:3535-3542.

Kitamura S, Maeda K, Wang Y and Sugiyama Y (2008) Involvement of multiple transporters in the hepatobiliary transport of rosuvastatin. *Drug Metab Dispos* **36**:2014-2023.

Lai XS, Yang LP, Li XT, Liu JP, Zhou ZW and Zhou SF (2009) Human CYP2C8: structure, substrate specificity, inhibitor selectivity, inducers and polymorphisms. *Curr Drug Metab* **10**:1009-1047.

Lai Y, Varma M, Feng B, Stephens JC, Kimoto E, El-Kattan A, Ichikawa K, Kikkawa H, Ono C, Suzuki A, Suzuki M, Yamamoto Y and Tremaine L (2012) Impact of drug transporter pharmacogenomics on pharmacokinetic and pharmacodynamic variability - considerations for drug development. *Expert Opin Drug Metab Toxicol* **8**:723-743.

Li R, Barton HA and Varma MV (2014) Prediction of pharmacokinetics and drug-drug interactions when hepatic transporters are involved. *Clin Pharmacokinet*:In Press.

Liu L and Pang KS (2005) The roles of transporters and enzymes in hepatic drug processing. *Drug Metab Dispos* **33**:1-9.

Lundquist P, Loof J, Sohlenius-Sternbeck AK, Floby E, Johansson J, Bylund J, Hoogstraate J, Afzelius L and Andersson TB (2014) The impact of solute carrier (SLC) drug uptake transporter loss in human and rat cryopreserved hepatocytes on clearance predictions. *Drug Metab Dispos* **42**:469-480.

Maeda K, Ikeda Y, Fujita T, Yoshida K, Azuma Y, Haruyama Y, Yamane N, Kumagai Y and Sugiyama Y (2011) Identification of the rate-determining process in the hepatic clearance of atorvastatin in a clinical cassette microdosing study. *Clin Pharmacol Ther* **90**:575-581.

Mazzu AL, Lasseter KC, Shamblen EC, Agarwal V, Lettieri J and Sundaresen P (2000) Itraconazole alters the pharmacokinetics of atorvastatin to a greater extent than either cerivastatin or pravastatin. *Clin Pharmacol Ther* **68**:391-400.

Menochet K, Kenworthy KE, Houston JB and Galetin A (2012) Use of mechanistic modeling to assess interindividual variability and interspecies differences in active uptake in human and rat hepatocytes. *Drug Metab Dispos* **40**:1744-1756.

Niemi M, Neuvonen PJ, Hofmann U, Backman JT, Schwab M, Lutjohann D, von Bergmann K, Eichelbaum M and Kivisto KT (2005) Acute effects of pravastatin on cholesterol synthesis are associated with SLCO1B1 (encoding OATP1B1) haplotype *17. *Pharmacogenet Genomics* **15**:303-309.

Niemi M, Pasanen MK and Neuvonen PJ (2011) Organic anion transporting polypeptide 1B1: a genetically polymorphic transporter of major importance for hepatic drug uptake. *Pharmacol Rev* **63**:157-181.

Nishizato Y, Ieiri I, Suzuki H, Kimura M, Kawabata K, Hirota T, Takane H, Irie S, Kusuhara H, Urasaki Y, Urae A, Higuchi S, Otsubo K and Sugiyama Y (2003) Polymorphisms of OATP-C (SLC21A6) and OAT3 (SLC22A8) genes: consequences for pravastatin pharmacokinetics. *Clin Pharmacol Ther* **73**:554-565.

Obach RS, Walsky RL, Venkatakrishnan K, Gaman EA, Houston JB and Tremaine LM (2006) The utility of in vitro cytochrome P450 inhibition data in the prediction of drug-drug interactions. *J Pharmacol Exp Ther* **316**:336-348.

Paine MF, Hart HL, Ludington SS, Haining RL, Rettie AE and Zeldin DC (2006) The human intestinal cytochrome P450 "pie". *Drug Metab Dispos* **34**:880-886.

Pang KS and Rowland M (1977) Hepatic clearance of drugs. II. Experimental evidence for acceptance of the "well-stirred" model over the "parallel tube" model using lidocaine in the perfused rat liver in situ preparation. *J Pharmacokinet Biopharm* **5**:655-680.

Prueksaritanont T, Chu X, Evers R, Klopfer S, Caro L, Kothare P, Dempsey C, Rasmussen S, Houle R and Chan G (2014) Pitavastatin is a more sensitive and selective OATP1B clinical probe than rosuvastatin. *Br J Clin Pharmacol*.

Shitara Y, Horie T and Sugiyama Y (2006) Transporters as a determinant of drug clearance and tissue distribution. *Eur J Pharm Sci* **27**:425-446.

Shitara Y and Sugiyama Y (2006) Pharmacokinetic and pharmacodynamic alterations of 3-hydroxy-3-methylglutaryl coenzyme A (HMG-CoA) reductase inhibitors: drug-drug interactions and interindividual differences in transporter and metabolic enzyme functions. *Pharmacol Ther* **112**:71-105.

Tomita Y, Maeda K and Sugiyama Y (2013) Ethnic variability in the plasma exposures of OATP1B1 substrates such as HMG-CoA reductase inhibitors: a kinetic consideration of its mechanism. *Clin Pharmacol Ther* **94**:37-51.

USFDA (2012) Drug interaction studies - study design, data analysis, implications for dosing, and labeling recommendations. *Center for Drug Evaluation and Research (CDER)*.

van Giersbergen PL, Treiber A, Schneiter R, Dietrich H and Dingemanse J (2007) Inhibitory and inductive effects of rifampin on the pharmacokinetics of bosentan in healthy subjects. *Clin Pharmacol Ther* **81**:414-419.

Varma MV, Lai Y, Feng B, Litchfield J, Goosen TC and Bergman A (2012) Physiologically based modeling of pravastatin transporter-mediated hepatobiliary disposition and drug-drug interactions. *Pharm Res* **29**:2860-2873.

Varma MV, Lai Y, Kimoto E, Goosen TC, El-Kattan AF and Kumar V (2013a) Mechanistic modeling to predict the transporter- and enzyme-mediated drug-drug interactions of repaglinide. *Pharm Res* **30**:1188-1199.

Varma MV, Lin J, Bi YA, Rotter CJ, Fahmi OA, Lam JL, El-Kattan AF, Goosen TC and Lai Y (2013b) Quantitative prediction of repaglinide-rifampicin complex drug interactions using dynamic and static mechanistic models: delineating differential CYP3A4 induction and OATP1B1 inhibition potential of rifampicin. *Drug Metab Dispos* **41**:966-974.

Varma MV, Scialis RJ, Lin J, Bi YA, Rotter CJ, Goosen TC and Yang X (2014) Mechanism-based pharmacokinetic modeling to evaluate transporter-enzyme interplay in drug interactions and pharmacogenetics of glyburide. *AAPS J* **16**:736-748.

Watanabe T, Kusuhara H, Maeda K, Shitara Y and Sugiyama Y (2009) Physiologically based pharmacokinetic modeling to predict transporter-mediated clearance and distribution of pravastatin in humans. *J Pharmacol Exp Ther* **328**:652-662.

Yoshida K, Maeda K and Sugiyama Y (2012) Transporter-mediated drug--drug interactions involving OATP substrates: predictions based on in vitro inhibition studies. *Clin Pharmacol Ther* **91**:1053-1064.

Zamek-Gliszczynski MJ, Lee CA, Poirier A, Bentz J, Chu X, Ellens H, Ishikawa T, Jamei M, Kalvass JC, Nagar S, Pang KS, Korzekwa K, Swaan PW, Taub ME, Zhao P, Galetin A and International Transporter C (2013) ITC recommendations for transporter kinetic parameter estimation and translational modeling of transport-mediated PK and DDIs in humans. *Clin Pharmacol Ther* **94**:64-79.

**LEGENDS FOR FIGURES:**

Figure 1. *In vitro-in vivo* extrapolation of hepatic intrinsic clearance of ten OATP1B1 substrate drugs. *In vitro* hepatic intrinsic clearance was calculated using extended clearance equation assuming $SF_{active}$ of unity (A) and geometric mean value (B). *In vitro* intrinsic clearance was significantly underpredicted when the SCHH and HLM data were directly adopted ($SF_{active}$ of unity) in extended clearance equation. After applying geometric mean $SF_{active}$ of 10.6, 60% drugs are within 2-fold and 70% within 3-fold of the observed values. Data points represent SCHH data from hepatocyte lot BD310 (△), lot 109 (◇) lot Hu4168 (○) and the mean of three lots (—). Diagonal solid and dashed lines represent unity and 2-fold error, respectively. A-atorvastatin; B-bosantan; C-cerivastatin; F-fluvastatin; G-glyburide; P-pitavastatin; Pr-pravastatin; R-rosuvastatin; Re-repaglinide; V-valsartan.

Figure 2. Observed versus predicted change in systemic exposure of the OATP1B1 substrate drugs when administered with (A) cyclosporine, (B) gemfibrozil, (C) rifampicin and (D) itraconazole or clarithromycin. Data points represent AUCR (circles), R-value (solid diamonds), and the change in overall hepatic intrinsic clearance (dash line). Diagonal solid and dashed lines represent unity and 2-fold error, respectively. *n is number of combinations evaluated and percentage represents number of predicted AUCRs within 2-fold of the observed AUCR.

Figure 3. Observed versus predicted AUCR of 62 DDI combinations using the extended net-effect model, considering the scaling factor for active uptake of (A) unity, (B) geometric mean and (C) drug-specific value. FN and FP represent false negative and false positive predictions, respectively. Data points represent DDIs with cyclosporine (solid squares), gemfibrozil

(diamonds), rifampicin (circles) and itraconazole or clarithromycin (solid triangles). Diagonal solid and dashed lines represent unity and 2-fold error, respectively.

Figure 4. Scattered plot of observed AUCR and predicted change in free liver-to-plasma ratio. Dashed vertical and horizontal lines represent no change in plasma AUC and $Kp_{uu}$, respectively. Interactions were classified based on the direction of change in AUCR and $Kp_{uu}$. Class A (+,+), increase in AUC and $Kp_{uu}$; Class B (+,−), increase in AUC and decrease in $Kp_{uu}$; Class C (−,−), decrease in AUC and $Kp_{uu}$; Class D (−,+), decrease in AUC and increase in $Kp_{uu}$. Data points represent DDIs with cyclosporine (solid squares), gemfibrozil (diamonds), rifampicin (circles) and itraconazole or clarithromycin (solid triangles).

Table 1. Summary of input parameters for victim and perpetrator drugs used in the mechanistic model-based predictions of transporter- and CYP-based DDIs.[†]

| Victim drug | Observed plasma CL (mL/min/kg)[a] | Plasma CLr (mL/min/kg)[a] | Fg | Plasma fu | Rb | *In vivo* $CL_{int,h}$ (mL/min/kg)[b] | $PS_{active}$ (µL/min/$10^6$ cells)[c] | $PS_{pd}$ (µL/min/$10^6$ cells)[c] | $CL_{int,HLM}$ (µL/min/mg)[d,e] | $fm_{CYP3A4}$[d] | $CL_{int,bile}$ (µL/min/$10^6$ cells)[c] | $SF_{active}$ | $Kp_{uu}$ |
|---|---|---|---|---|---|---|---|---|---|---|---|---|---|
| Atorvastatin | 7.8 | 0 | 0.60 | 0.024 | 0.61 | 853 | 12.4 | 8.6 | 59.8 | 0.85 | 1.5 | 32.6 | 12.0 |
| Bosantan | 2.1 | 0 | 0.98 | 0.037 | 0.66 | 67 | 35.5 | 10.0 | 20.0 | 1.00 | 2.0 | 1.1 | 2.5 |
| Cerivastatin | 2.9 | 0 | 0.74 | 0.014 | 0.76 | 254 | 16.8 | 17.5 | 31.9 | 0.45[g] | 0.2 | 12.5 | 7.4 |
| Fluvastatin | 8.7 | 0 | 1.00 | 0.008 | 0.57 | 4141 | 30.7 | 15.3 | 29.4 | 0.46[h] | 2.9 | 101.8 | 104.1 |
| Glyburide | 0.8 | 0 | 0.97 | 0.021 | 0.58 | 42 | 15.8 | 5.3 | 53.0 | 0.53[h] | 0.0 | 1.0 | 0.8 |
| Pitavastatin | 5.7[a] | 0 | 1.00 | 0.025 | 0.58 | 434 | 34.8 | 11.1 | 15.0 | 0.00[h] | 0.7[f] | 12.3 | 24.5 |
| Pravastatin | 13.5 | 6.3 | 1.00 | 0.47 | 0.56 | 40 | 1.4 | 0.4 | - | - | 0.4[f] | 19.4 | 34.5 |
| Rosuvastatin | 11.7 | 3.3 | 1.00 | 0.12 | 0.69 | 171 | 9.1 | 1.2 | - | - | 2.8[f] | 9.2 | 21.1 |
| Repaglinide | 7.8 | 0 | 0.94 | 0.015 | 0.62 | 1326 | 35.5 | 22.0 | 131.0 | 0.29[g] | 0.1 | 18.7 | 9.1 |
| Valsartan | 0.5 | 0.15 | 1.00 | 0.01 | 0.55 | 35 | 2.5 | 1.0 | - | - | 0.9 | 9.9 | 13.6 |

| Perpetrator drug | Ka | Fa | Fg | Plasma fu | Rb | fu,gut | Interaction potential |
|---|---|---|---|---|---|---|---|
| Cyclosporine | 0.025 | 0.86 | 0.48 | 0.068 | 1.36 | 1 | reversible inhibition of OATP1B1 (Ki=0.014µM), CYP3A4 (Ki=2µM), MRP2 (Ki=4.1µM) and BCRP (Ki=6.7µM) |
| Gemfibrozil | 0.05 | 1 | 1 | 0.03 | 0.82 | 1 | reversible inhibition of OATP1B1 (Ki=2.54µM) and OAT3 (Ki=3.4µM) |
| Gemfibrozil-1-O-b-glucuronide | | | | 0.115 | 1.0 | | reversible inhibition of OATP1B1 (Ki=7.9µM) and OAT3 (Ki=9.9µM); time-dependent inhibition of CYP2C8(KI=10.1µM, $K_{inact}$=12.6/h) |
| Rifampicin | 0.0085 | 1 | 0.99 | 0.15 | 0.9 | 0.15 | reversible inhibition of OATP1B1 (Ki=0.9µM); induction of CYP3A4 (Emax=49.5, $EC_{50}$=0.23µM) |
| Clarithromycin | 0.04 | 1 | 0.69 | 0.18 | 1.0 | 1 | reversible inhibition of OATP1B1 (Ki=8.3µM); time-dependent inhibition of CYP3A4 (KI=14µM, $K_{inact}$=1.7/h) |
| Itraconazole | 0.01 | 0.85 | 0.83 | 0.036 | 0.58 | 0.016 | reversible inhibition of CYP3A4 (Ki=0.0013µM) |
| 4-OH-Itraconazole | | | | 0.021 | 1.0 | | reversible inhibition of CYP3A4 (Ki=0.014µM) |

[†]References provided in Supplementary Table S5

[a]intravenous clearance, except for pitavastatin, in which case clearance was obtained by correcting the oral clearance with the estimated oral bioavailability [taken from Yoshida, et al. (Yoshida et al., 2012)]. [b]*in vivo* $CL_{int,h}$ was calculated using Eq. 15. [c]*in vitro* mean data from independent SCHH studies using three different hepatocyte lots (see Methods). [d]*in vitro* data based on substrate depletion in

human liver microsomes or recombinant CYPs (see Methods). No significant metabolism was observed for pravastatin, rosuvastatin and valsartan. [e]values corrected for microsomal binding. [f]biliary clearance was assumed to be mediated by BCRP (pitavastatin and rosuvastatin) and MRP2 (pravastatin). [g]remaining fraction metabolism is associated with CYP2C8. [h]remaining fraction metabolism is associated with CYP2C9.

Table 2. Statistical comparison of R-value and model-based predictions of DDIs assuming different scaling factor for active hepatic uptake.

| DDIs with | n | R-value | | | | $SF_{active}$ = 1 | | | | $SF_{active}$ = geometric mean (10.6) | | | | $SF_{active}$ = drug-specific | | | |
|---|---|---|---|---|---|---|---|---|---|---|---|---|---|---|---|---|---|
| | | FN↔ | RMSE | AFE | % within 2-fold | FN↔ | RMSE | AFE | % within 2-fold | FN↔ | RMSE | AFE | % within 2-fold | FN↔ | RMSE | AFE | % within 2-fold |
| Cyclosporine | 12 | 0 | 4.6 | 1.6 | 75 | 2 | 6.2 | 2.9 | 42 | 0 | 4.8 | 1.8 | 67 | 0 | 4.3 | 1.6 | 83 |
| Gemfibrozil | 15 | 3 | 4.8 | 2.2 | 46 | 0 | 3.3 | 1.8 | 60 | 0 | 2.0 | 1.4 | 87 | 0 | 2.4 | 1.4 | 93 |
| Rifampicin | 22 | 0* | 3.0* | 1.6* | 70* | 2 | 3.1 | 1.8 | 54 | 3 | 1.9 | 1.4 | 86 | 2 | 1.4 | 1.3 | 95 |
| Itraconazole and clarithromycin | 13 | 2θ | 1.5θ | 1.5θ | 75θ | 6 | 0.6 | 1.3 | 100 | 5 | 0.5 | 1.3 | 100 | 5 | 0.5 | 1.3 | 100 |
| All | 62 | 5*,θ | 4.2*,θ | 1.9*,θ | 63*,θ | 10 | 3.7 | 1.9 | 63 | 8 | 2.6 | 1.4 | 86 | 7 | 2.4 | 1.4 | 94 |

↔False negatives (FN) represent number of instances where the observed AUCR was ≥1.25 and the predicted AUCR was <1.25. For DDIs associated with rifampicin induction these cut-offs were defined at ≤0.8 (observed) and >0.8 (Predicted). Lower FN, RMSE and AFE values would indicate a better prediction. No false positives were predicted with this dataset.

*(n=12) R-value evaluation of rifampicin DDIs considered only cases with single dose rifampicin, where CYP3A4 induction is assumed negligible.

θ(n=4) R-value evaluation of clarithromycin DDIs only.

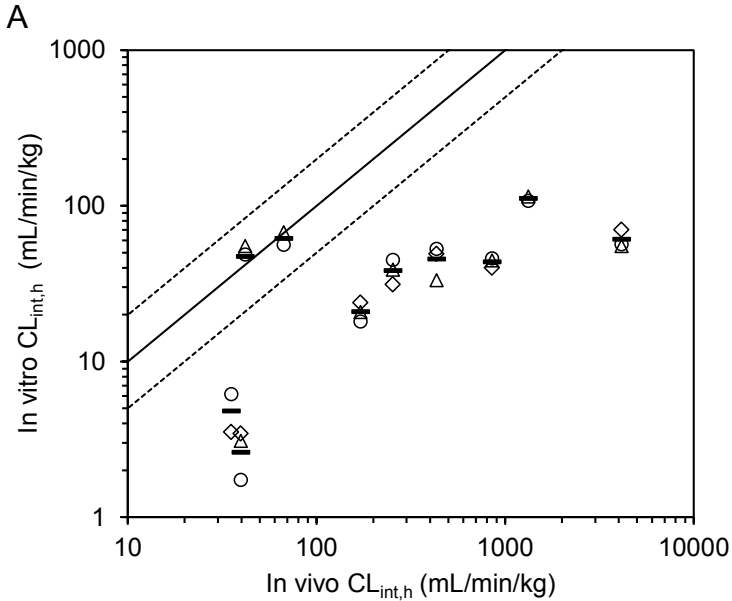


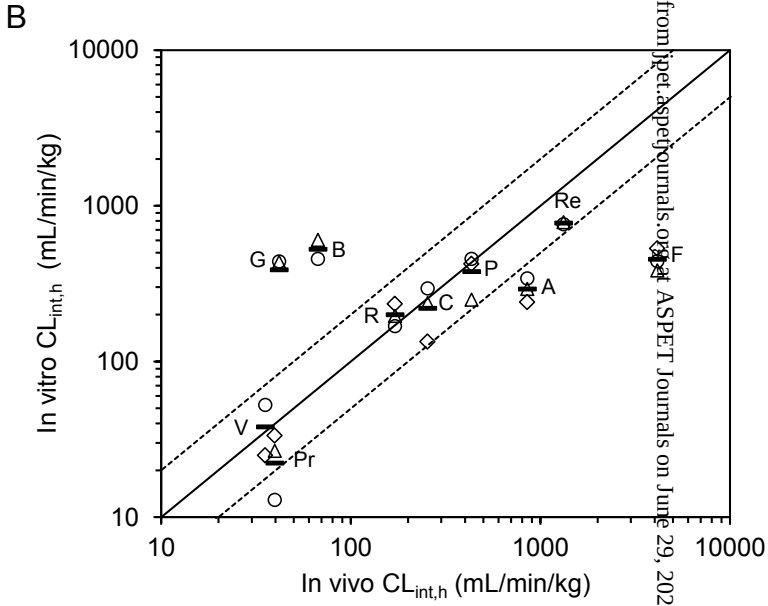




Figure 1

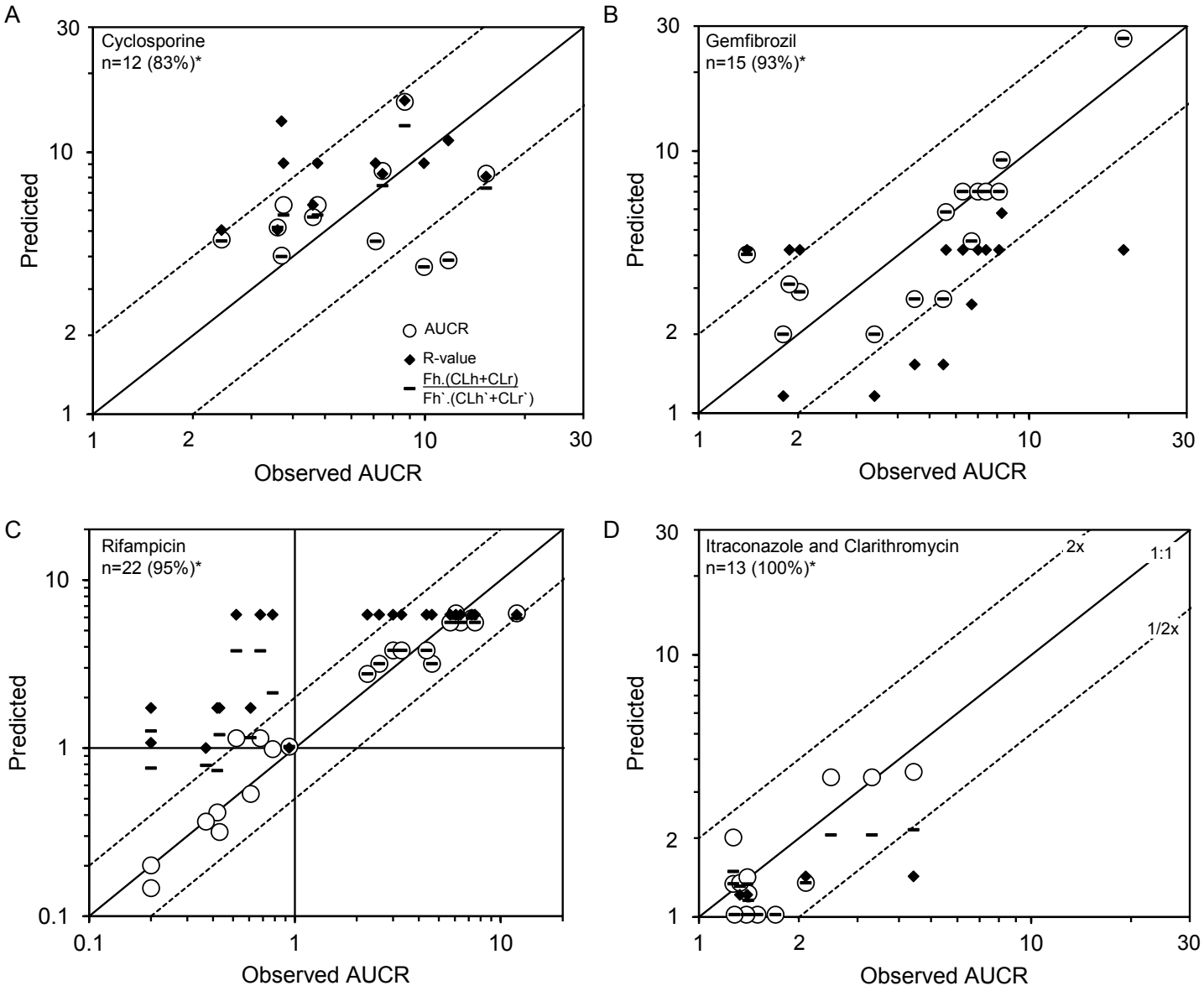
A
Cyclosporine
n=12 (83%)*
Predicted
Observed AUCR
AUCR
R-value
Fh.(CLh+CLr)
Fh`.(CLh`+CLr`)
B
Gemfibrozil
n=15 (93%)*
Predicted
Observed AUCR
C
Rifampicin
n=22 (95%)*
Predicted
Observed AUCR
D
Itraconazole and Clarithromycin
n=13 (100%)*
2x
1:1
1/2x
Predicted
Observed AUCR

Figure 2

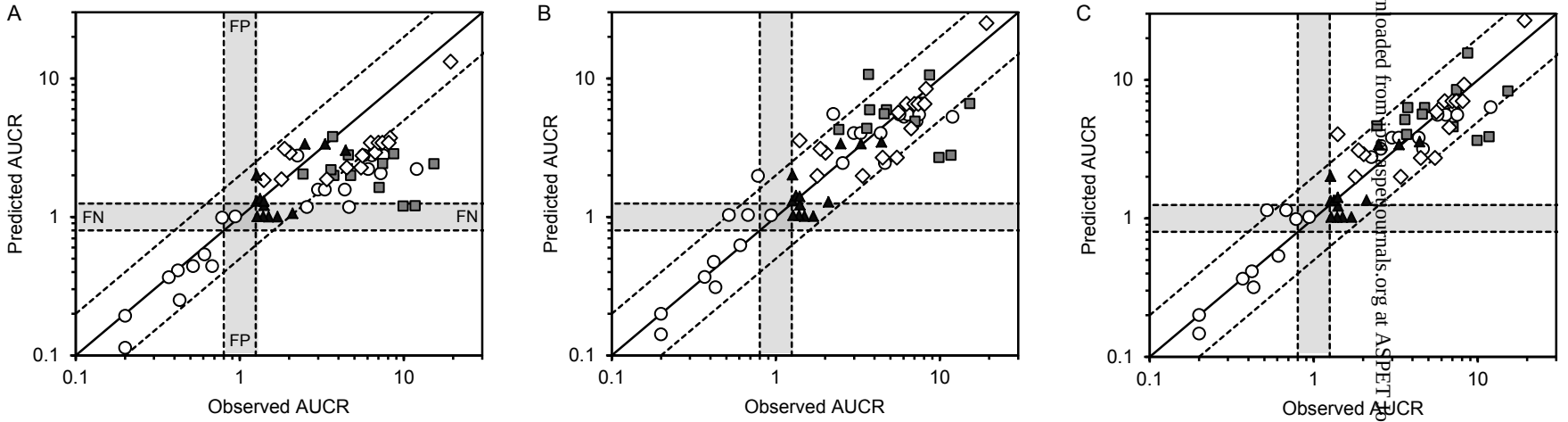


Figure 3

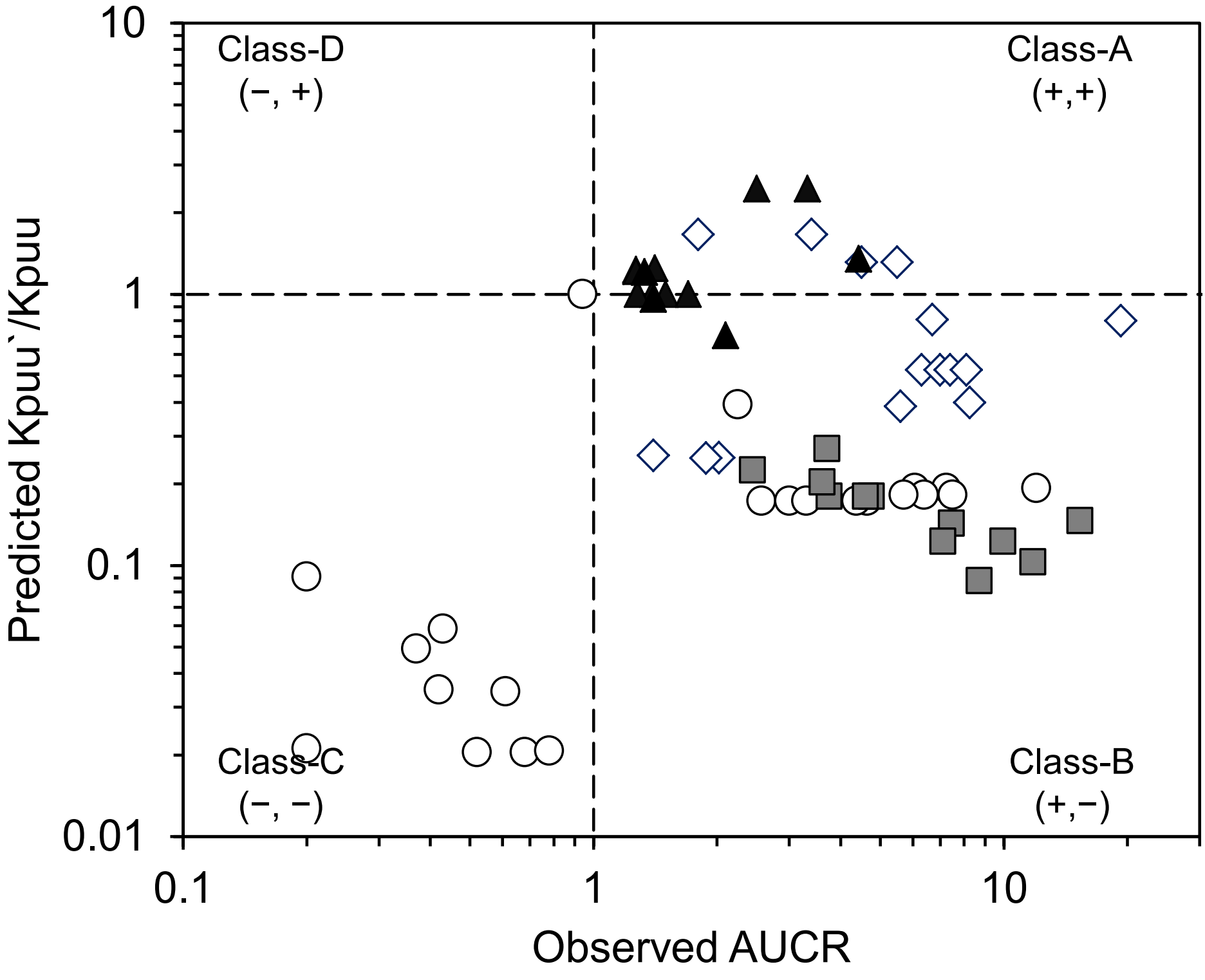
10
1
0.1
0.01
Class-D
(−, +)
Class-A
(+,+)
Class-C
(−, −)
Class-B
(+,−)
Predicted Kpuu`/Kpuu
0.1
1
10
Observed AUCR

Figure 4